The FEBS Journal

FEBS PRESS science publishing by scientists

Cytoplasmic localization of Mdm2 in cells expressing mutated NPM is mediated by p53

Dita Strachotová[1], Aleš Holoubek[2], Kateřina Wolfová[2], Barbora Brodská[2] and Petr Heřman[1]

1 Faculty of Mathematics and Physics, Institute of Physics, Charles University, Prague 2, Czech Republic
2 Department of Proteomics, Institute of Hematology and Blood Transfusion, Prague 2, Czech Republic

Keywords
acute myeloid leukaemia; FRET-FLIM; Mdm2; nucleophosmin mutation; p53

Correspondence
P. Heřman, Faculty of Mathematics and Physics, Institute of Physics, Charles University, Ke Karlovu 5, 121 16 Prague 2, Czech Republic
Tel: +420 95155 1461
E-mail: herman@karlov.mff.cuni.cz
and
B. Brodská, Department of Proteomics, Institute of Hematology and Blood Transfusion, U Nemocnice 1, 128 20 Prague 2, Czech Republic
Tel: +420 221 977 354
E-mail: brodska@uhkt.cz

Dita Strachotová and Aleš Holoubek contributed equally to this article

(Received 27 October 2022, revised 2 April 2023, accepted 28 April 2023)

doi:10.1111/febs.16810

Specific C-terminal nucleophosmin (NPM) mutations are related to the acute myeloid leukaemia and cause mistargeting of mutated NPM (NPMmut) to the cytoplasm. Consequently, multiple NPM-interacting partners, e.g., the tumour suppressor p53, become also mislocalized. We found that ubiquitin ligase Mdm2 mislocalizes to the cytoplasm in the presence of NPMmut as well. Since p53 interacts with Mdm2, we searched for the NPMmut-p53-Mdm2 complex and interactions of its constituents in live cells and cell lysates using fluorescently tagged proteins, fluorescence lifetime imaging and immunoprecipitation. We proved existence of the ternary complex, which likely adopts a chain-like configuration. Interaction between Mdm2 and NPMmut was not detected, even under conditions of upregulated Mdm2 and p53 induced by Actinomycin D. We assume that p53 serves in the complex as a bridging link between Mdm2 and NPMmut. This conclusion was supported by disruption of the Mdm2–p53 interaction by Nutlin-3A, which resulted in relocalization of Mdm2 to the nucleus, while both NPMmut and p53 remained in the cytoplasm. Importantly, silencing of p53 also prevented mislocalization of Mdm2 in the presence of NPMmut.

Introduction

Specific C-terminal nucleophosmin (NPM) mutations are the most frequent acute myeloid leukaemia (AML)-related mutations [1]. AML patients with isolated NPM mutation and normal karyotype belong to the group with good prognosis of standard intensive treatment protocol [2]. However, these mutations are frequently accompanied by other mutations worsening the prognosis, e.g., Flt3-ITD and/or DNMT3A. The NPM mutations affect the wild-type (NPMwt) C-terminal sequence containing the nucleolar localization signal and cause aberrant localization of mutated NPM (NPMmut) to the cytoplasm [1]. Consequently, multiple NPMmut-interacting partners are targeted to the cytoplasm [3,4]. Among these, tumour suppressor

Abbreviations
3FF, three-colour-FRET-FLIM; ActD, actinomycin D; AML, acute myeloid leukaemia; C_Mdm2, Mdm2 labelled with Cerulean; C_NPMmut, mutated NPM labelled with Cerulean; C_NPMwt, wild-type NPM labelled with Cerulean; FLIM, fluorescence lifetime imaging; FP, fluorescent protein; FRET, Förster resonance energy transfer; G_NPMwt, wild-type NPM labelled with eGFP; NCL, nucleolin; NPM, nucleophosmin; NPMmut, mutated nucleophosmin; NPMwt, wild-type nucleophosmin; R_NPMmut, mutated NPM labelled with mRFP1; R_NPMwt, wild-type NPM labelled with mRFP1; R_p53, p53 labelled with mRFP1; V_Mdm2, Mdm2 labelled with mVenus; V_NPMmut, mutated NPM labelled with mVenus; V_NPMwt, wild-type NPM labelled with mVenus.

p53 has recently been proven to interact with both wt and mutated NPM and is consequently found in the cytoplasm of NPMmut-expressing cells [5]. This probably causes impaired p53 signalization and delayed/inhibited p53-dependent apoptosis [6]. Drugs preventing the cytoplasmic p53 localization may, therefore, help to cure AML with NPM mutation. In our previous work, we tested specific effect of the putative NPM-oligomerization inhibitor, NSC348884, as well as the inhibitor of the nuclear exporter Crm1, Selinexor, exerted on apoptosis of the cells with NPM mutation [5,7]. However, NSC348884 was found ineffective as the NPM-oligomerization inhibitor. Instead, it caused apoptosis by affecting mechanisms of cell adhesion. Similarly, Selinexor targets NPMmut and p53 to the nucleus and causes apoptosis; however, this process is not NPMmut specific. In this work, we focused on the p53-interacting partner and its negative regulator, the human E3-ubiquitin ligase Mdm2 (hdm2), regulating p53 degradation.

Mdm2 tightly interacts with p53 in mouse fibroblasts and in many human cancer-derived cell lines [8–11]. This interaction mediates stepwise p53 ubiquitinylation. Subsequently, Mdm2 with Mdm4 facilitates degradation of polyubiquitinylated p53 by proteasome [12–14]. The interaction between N termini of Mdm2 and p53 is accompanied by inhibition of p53 transcriptional activity [15]. Interaction of their central parts allows nuclear association of ubiquitin to p53 [8,9,16,17]. The latter modification is followed by partial relocalization of the ubiquitinylated p53 to the cytoplasm and its recognition by the proteasome [18]. Simultaneously, p53 binding to the Mdm2 promoter activates Mdm2 transcription which represents a negative feedback loop in the regulation of both proteins [13]. Dynamic regulation of p53 occurs mainly at the protein level without correlation between its mRNA and the protein expression [19]. p53 is rather unstable with half-life ranging from 5 to 30 min in normal cells [20]. Its stabilization and activation after a genotoxic stress frequently induced by cytotoxic drugs results in a significant increase of p53 levels. Importantly, oligomeric state of p53 is critical for its Mdm2-induced degradation [16] as well as for its transcription-regulating association with DNA [21]. Mdm2 is often overexpressed in many cancers, including leukaemias. This leads to massive p53 degradation and extremely low p53 levels resulting in impaired apoptosis and deregulated proliferation [22–24].

Formation of the Mdm2-p53 complex is affected by many interactions, especially by interactions with tumour suppressor p19Arf/p14Arf and NPM [25]. p19Arf sequestered by NPM in nucleoli of intact cells is released to bind Mdm2 under stress conditions. As a consequence, p53 is stabilized, its activity increases and cells are driven to apoptosis [25]. AML-related NPM mutation targets p19Arf in the cytoplasm, where p19Arf is not protected from degradation and cannot initiate the p53-dependent response to stress [25]. Regulation of p53 and Mdm2 levels by NPM has been widely described and includes both direct protein interactions and regulation of transcription facilitated by NPM interaction with transcription factors [3,26]. Enhanced Mdm2 and p53 expression was found in NPM overexpressing cells. Silencing of NPM led to decreased p53 activity and stability [10,11].

Nucleoplasmic relocalization of NPM was detected after UV-induced stress. Under these conditions, NPM transiently binds Mdm2, thus releasing p53 from its interaction with Mdm2 [27–29]. UV-induced Mdm2–NPM interaction was found to be associated with a specific SIRT7-mediated NPM deacetylation followed by the p53 stabilization [28]. The Mdm2–NPM interaction was reported also in cells treated with proteasome inhibitor MG132 [27]. Increased Mdm2 transcript level correlated with NPMmut presence in AML cell lines as well as in blasts of AML patients [26]. Higher Mdm2 transcription was accompanied by a higher expression of the Mdm2-binding transcription factor MEF/Elf4, which interacted with NPMwt but it did not interact with NPMmut. This indicates competitive binding of NPMwt to the MEF/Elf4 [26].

Altogether, mutual interactions have been detected between all proteins of Mdm2–p53–NPM complex, at least under specific conditions. To the best of our knowledge, nothing is known about the potential role of NPM mutation in the modulation of the p53–Mdm2 interaction and its possible consequences in leukemogenesis. The existence of the ternary Mdm2–p53–NPM complex with a dynamic exchange of its constituents and its role in the regulation network is completely elusive. We, therefore, established a Fluorescence lifetime imaging (FLIM)-based approach for detection of all three protein constituents within the Mdm2–p53–NPM complex in live cells and for characterization of their mutual proximity.

In cells with NPM mutation, the signalization pathways based on the NPM–p53–Mdm2 axis are deregulated by the cytoplasmic delocalization of p53 [5], which might contribute to the NPMmut-induced leukemogenesis. Impairment of the complex stability by proper inhibitors could, therefore, release p53 for the induction of apoptosis and restoration of the Mdm2 nuclear localization. We, therefore, analysed interactions within the NPM–p53–Mdm2 complex related to the NPM mutation in cell lysates and live HEK-293T cells. Effect of the Mdm2–p53 interaction inhibitor Nutlin-3A, and the

genotoxic stress inductor Actinomycin D (ActD) on the interactions between each pair of the proteins in the complex was investigated. Results were verified on a panel of AML cell lines.

Results

Mdm2 localizes to the cytoplasm together with NPMmut

We assume that the complex signalization pathways based on the NPM–p53–Mdm2 axis are seriously dysregulated in cells with the AML-related NPM mutation. In order to evaluate the impact of NPMmut on all members of the regulation axis, we performed comparative cellular localization experiment on HEK-293T cells transfected with plasmids for expression of mVenus-labelled NPMwt and NPMmut (V_NPMwt and V_NPMmut). The cells were further cotransfected with mRFP1-tagged p53 (R_p53) and Cerulean-labelled Mdm2 (C_Mdm2). All three fluorescent tags are spectrally well separated and their subcellular colocalization can be examined by fluorescence microscopy. The result is shown in Fig. 1. In Fig. 1A, we can see that while in the presence of nucleoli-localized V_NPMwt both R_p53 and C_Mdm2 stay correctly mainly in the cell nuclei [30], the localization pattern in the presence of V_NPMmut is clearly different. Both C_Mdm2 and R_p53 are relocalized to the cytoplasm. As we have reported earlier [5], the cytoplasmic mislocalization of NPMmut causes extensive relocalization of its binding partner p53. Figure 1A documents similar delocalization of C_Mdm2 in the presence of V_NPMmut. To check for a potential bias caused by the extrinsic label and overexpression of exogenous p53, we repeated the experiment relying on endogenous p53 in cells cotransfected with only C_Mdm2 and V_NPMmut. The localization of endogenous p53 was visualized by AlexaFluor555 immunostaining after fixation of the transfected cells. As seen in Fig. 1B, for cells expressing V_NPMmut, we obtained essentially the same result as in Fig. 1A, that is, cytoplasmic relocalization of Mdm2. We can see that endogenous p53 accompanies both NPMmut and Mdm2 to the cytoplasm in samples expressing NPMmut. Labelling of NPMmut by different fluorescent tags neither changed the observed pattern (data not shown).

The localization experiments suggest a tight correlation between the cellular expression of NPMmut and the cytoplasmic mislocalization of Mdm2. It is, therefore, important to search for the mechanism of the Mdm2 relocalization. This process could be facilitated by the interaction of Mdm2 with NPMmut, similarly as NPMmut was found to translocate both NPMwt and p53 to the cytoplasm [5,31]. Since the interaction between p53 and both NPMwt and NPMmut was documented [5,32], it seems reasonable to search for the existence of the direct NPM–Mdm2 interaction and the NPM–p53–Mdm2 complex, with the emphasis on the role of the NPM mutation. Answers to these questions could identify potential targets for reverting the regulation misbalance and pave the road for AML treatment.

Three-colour FRET-FLIM can detect ternary complexes in live cells

In order to search for the NPM–p53–Mdm2 ternary complex in live cells, we have chosen three-colour labelling scheme where different constituents of the ternary complex are each labelled with a specific spectrally separable fluorescent protein (FP). Then, mutual interactions within the complex can be simultaneously determined by FRET-FLIM using three different donor–acceptor pairs (Fig. 2). We call the method three-colour-FRET-FLIM (3FF). Similar approaches have been successfully used for detection of multimolecular complexes and monitoring of their conformational changes [33–35]. In Fig. 2A, we can see that the cyan label serves as a FRET donor for the yellow and red acceptor. The yellow label has a dual role of being the acceptor for the cyan tag and the donor for the red one. The red FP is a common acceptor for the two other tags. Since the presence of FRET reflecting donor–acceptor proximity demonstrates itself by a decreased donor fluorescence lifetime, the photobleaching of the red acceptor should affect both the cyan and the yellow donor (Fig. 2A,B). Consequently, their lifetimes should increase [36]. Similarly, photobleaching of the yellow tag closes the FRET channel between the cyan and the yellow FPs and the lifetime of the cyan donor further increases (Fig. 2C). The outlined scenario can prove interaction among all three constituents of the ternary complex.

We validated the method on the well-characterized system consisting of NPM variants labelled with three different FPs and coexpressed in cells. NPM molecules are known to form higher oligomers, pentamers or decamers [37]. Using FRET-FLIM, we have previously confirmed a formation of mixed NPM complexes both for wild type (NPMwt) and the mutated form NPMmut [7,38]. The 3FF experiment with NPMwt labelled by Cerulean (C_NPMwt), mVenus (V_NPMwt) and mRFP1 (R_NPMwt) is shown in Fig. 2D–H.

As expected, all variants of NPMwt are colocalized mainly in nucleoli where they are supposed to form three-colour oligomeric NPM complex containing random mix of the "colored" monomers [7]. Indeed, we clearly detect FRET among all three donor–acceptor

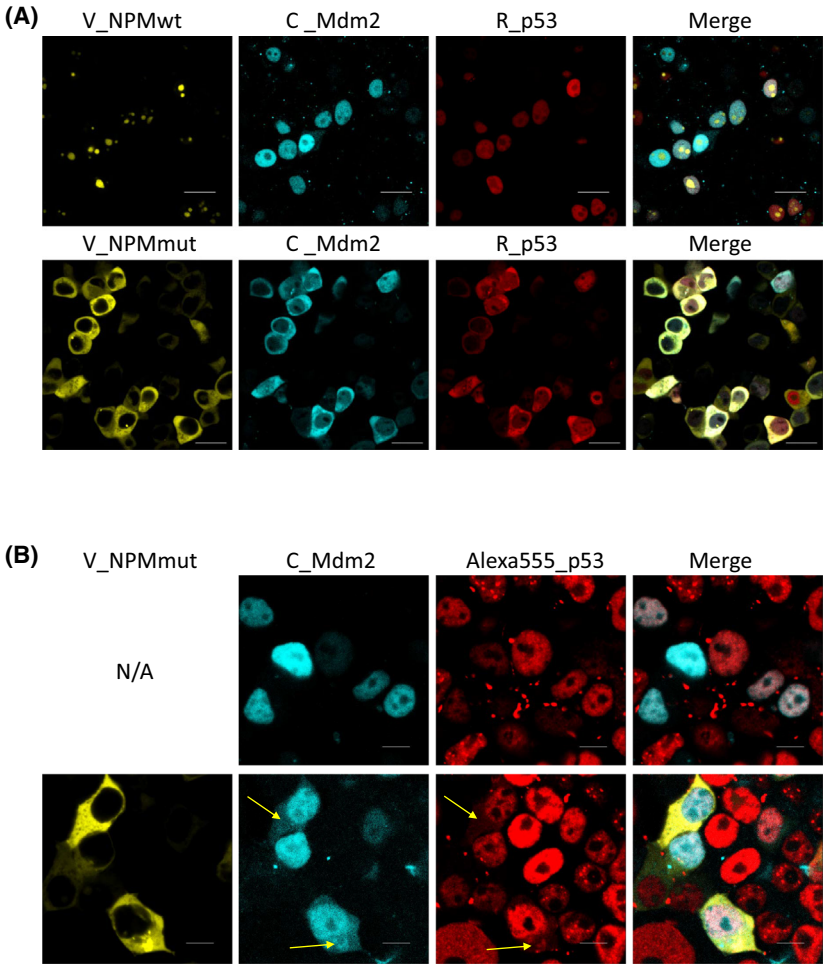

Fig. 1. Cellular localization of Mdm2 and p53 in the presence of exogenous variants of NPM in live HEK-293T cells. (A) Cells cotransfected with exogenous V_NPM, C_Mdm2 and R_p53. (1st row) – Localization of C_Mdm2 and R_p53 in the presence of V_NPMwt. (2nd row) – localization of C_Mdm2 and R_p53 in the presence of V_NPMmut. Bar is 20 μm, ($N = 5$). (B) Effect of endogenous p53. (1st row) – Cells transfected with C_Mdm2 only, (2nd row) – cells cotransfected with C_Mdm2 and V_NPMmut. Endogenous p53 is visualized by immunostaining with AlexaFluor555. Cytoplasmic localization of Mdm2 and p53 in the presence of NPMmut is marked by arrows. Bar is 10 μm ($N = 3$).

pairs. Specifically, fluorescence lifetime of C_NPMwt significantly increases after photodestruction of mRFP1 acceptor (Bleach1, R_NPMwt). Similar effect exerts the Bleach1 on the second donor mVenus. Additional bleach of V_NPMwt (Bleach2), which serves as a second acceptor of C_NPMwt, causes further increase of the

Fig. 2. Design and validation of the three-colour-FRET-FLIM (3FF) experiment. (A) Scheme of the experiment. Coloured circles represent proteins tagged with a specific FP, and grey circles are the proteins after photobleaching. FRET between each donor–acceptor pair is evaluated from the increase of the donor fluorescence lifetime upon the acceptor photodestruction. (B) Donor Cerulean or mVenus, acceptor mRFP1. (C) Donor Cerulean, acceptor mVenus. (D, E) Molecular proximity in the NPMwt multimer in live HEK-293T cells cotransfected with C_NPMwt, V_NPMwt and R_NPMwt. (D) Intensity images. Columns from left to right represent cyan, yellow and red spectral channels for detection of C_NPMwt, V_NPMwt and R_NPMwt fluorescence. Rows from top to bottom represent images of the initial triple-stained sample, images after mRFP1 photodestruction by 561 nm light and the images after additional photobleaching of mVenus by 514 nm radiation respectively. The photobleached areas are marked by the dashed line, bar is 10 μm. (E) FLIM images of C_NPMwt donor (the cyan spectral channel) in the presence of both V_NPMwt and R_NPMwt acceptors and after subsequent photodestruction of mRFP1 and mVenus, Bleach1 and Bleach2 respectively. (F) FLIM images of V_NPMwt donor (the yellow spectral channel) in the presence of the R_NPMwt acceptor and after its photobleaching (Bleach1). (G, H) Fluorescence lifetime distributions corresponding to the panels E and F respectively. Nucleolar areas for the histogram construction are marked by dashed lines. Experiments were performed in triplicates.

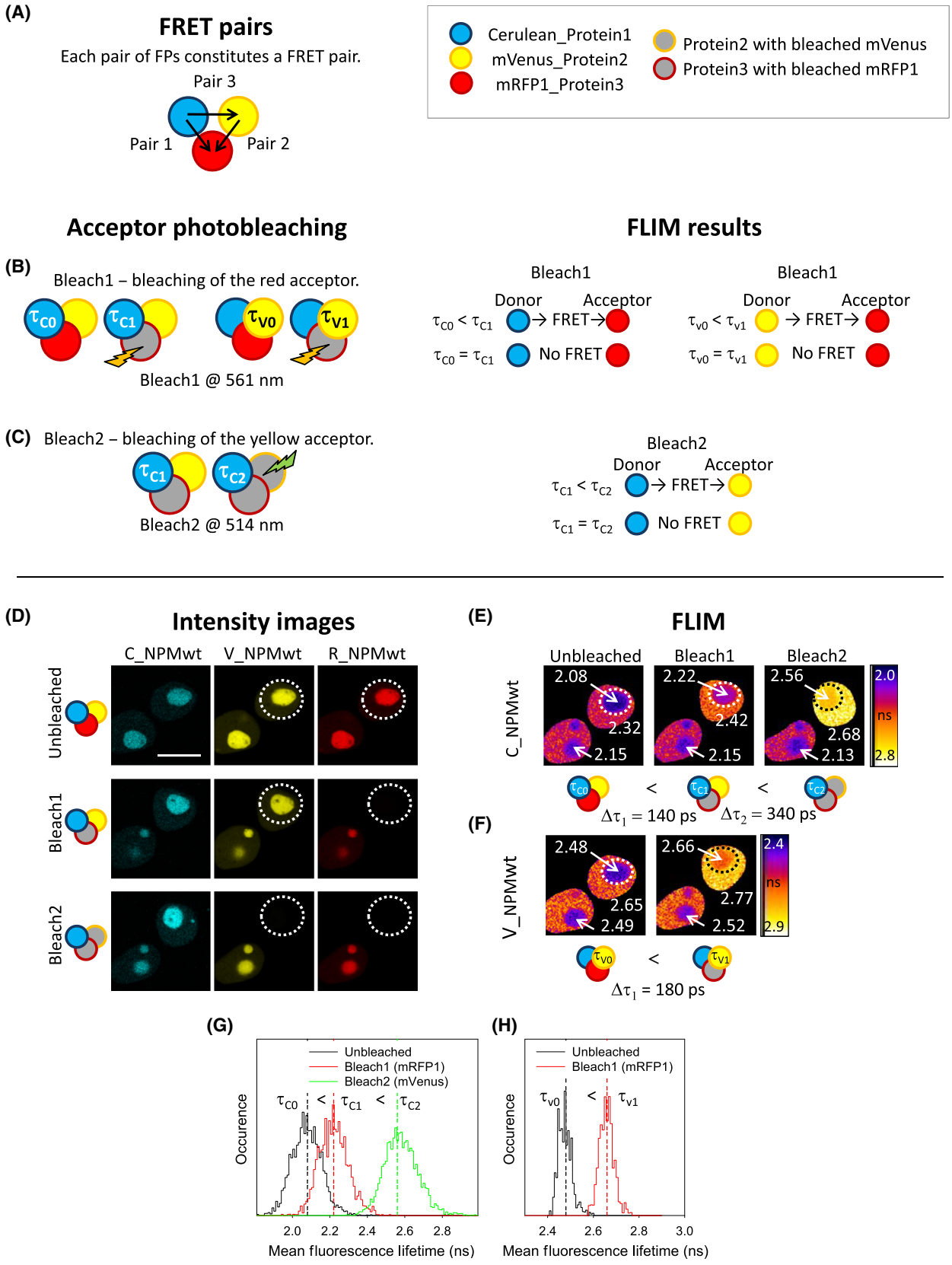

C_NPMwt lifetime. The results, therefore, clearly prove the presence of three opened FRET channels in the NPMwt oligomers, which documents simultaneous presence of all three colour variants of NPMwt in the complexes. Similar results were obtained for different combinations of cytoplasm-localized NPMmut colour variants (data not shown). The chosen labelling system is, therefore, well suited for the detection of ternary complexes by the 3FF method.

Complex NPMmut–p53–Mdm2 forms chain-like structure

Next, we applied the 3FF method for probing the suggested NPMmut–p53–Mdm2 complex and for searching for the direct Mdm2–NPMmut interaction. Figure 3 presents the 3FF experiment with HEK-293T cells cotransfected with Cerulean-labelled NPMmut (C_NPMmut), mVenus-labelled Mdm2 (V_Mdm2) and R_p53. Consistent with Fig. 1, the three proteins colocalize in the cytoplasm in the presence of NPMmut. We can see that after photodestruction of the mRFP1 acceptor, the emission lifetime of both Cerulean and mVenus donor increases (Fig. 3B–D). Statistical evaluation of repeats performed with several cell samples is shown in Fig. 3E. The observation witnesses for FRET between R_p53 and both C_NPMmut and V_Mdm2. Interaction between p53 and NPMmut detected by FRET has been already documented *in vivo* [5]. Nevertheless, despite expectations, we do not see any signs of NPMmut–Mdm2 interaction since the lifetime τ_{C1} of the C_NPMmut donor does not change upon photodestruction of the V_Mdm2 acceptor (Fig. 3B,D). Varied content of the exogenous Mdm2 and permutated three-colour labelling did not change this finding (data not shown). Therefore, we attempted to search for the Mdm2–NPMmut interaction in a double-labelled C_NPMmut-V_Mdm2 system (Fig. 3F-H). We can see that the lifetime histograms of C_NPMmut shown in Fig. 3H are independent of the presence or absence of V_Mdm2 and the result is, therefore, inconsistent with the close proximity of the donor and acceptor molecules required for the direct interaction. Statistical evaluation of repeats obtained with several independent cell samples and different protein tagging supports the conclusion (Fig. 3I).

The absence of FRET does not necessarily mean the absence of the short-range interaction, because under rather specific donor–acceptor orientation, the FRET could be weak or absent [36]. We, therefore, performed immunoprecipitation experiments to support the FLIM findings and mutual interactions of Mdm2, p53 and NPMwt/mut variants were searched in cell lysates. HEK-293T cells were transfected with C_Mdm2 and cotransfected either with mRFP1_p53 or with the mRFP1-labelled variants of NPM. Then, the cell lysates were analysed. Results are presented in Fig. 4. As suggested by our *in vivo* FLIM experiments, the interaction of exogenous Mdm2 with p53 was clearly detected in all samples (Fig. 4A). p53 also co-precipitated with both exogenous NPMwt and exogenous NPMmut (Fig. 4B). p53 was found to co-precipitate more with Mdm2 than with examined NPM variants, which confirms strong association between p53 and Mdm2 (Fig. 4B). Importantly, no signs of interaction between Mdm2 and NPMmut were detected (Fig. 4A), which fully supports our FLIM conclusions. In addition, neither endogenous NPMwt co-precipitated with Mdm2 (Fig. 4C) suggesting that absence of NPMmut–Mdm2 interaction is not caused by the mutation. The ability of Mdm2 to interact with p53 as well as its inability to interact with NPM was found independent of the used fluorescent tag as well (Fig. 4D). Consistent with literature, the Mdm2–

Fig. 3. Mutual interactions of Mdm2, NPMmut and p53 in live HEK-293T cells cotransfected by C_NPMmut, V_Mdm2 and R_p53. (A) Intensity images. Columns from left to right represent cyan, yellow and red fluorescence of C_NPMmut, V_Mdm2 and R_p53. Rows from top to bottom are images of the initial triple-labelled sample, images after mRFP1 photodestruction and images after additional photobleaching of mVenus. The bleached area is marked by the dashed line, bar is 20 μm. (B) FLIM images of C_NPMmut donor in the presence of both V_Mdm2 and R_p53 acceptors (left), after photodestruction of mRFP1 by 561 nm light (middle, Bleach1) and mVenus by 514 nm light (right, Bleach2). (C) Fluorescence lifetime images of V_Mdm2 donor in the presence of R_p53 acceptor (left) and after mRFP1 photobleaching (right, Bleach1). (D) Fluorescence lifetime histograms corresponding to the bleached area in panels B and C respectively. (E) Paired *t*-test for independent repeats of FRET-FLIM experiments comparing fluorescence lifetimes before and after the acceptor photobleaching. The graph contains data from different cell samples and three different donor–acceptor pairs. Lifetime changes are significant compared to the control. (F) Intensity images of C_NPMmut and V_Mdm2 before and after photobleaching of V_Mdm2. The bleached area is marked by the dashed line, bar is 10 μm. (G) FLIM images of the C_NPMmut before (left) and after (right) photodestruction of mVenus. (H) Lifetime histograms of the area marked in panel G before (black line) and after (red line) the photobleaching. Schematic representations refer to Fig. 2. (I) Paired *t*-test for independent repeats of FRET-FLIM experiments comparing fluorescence lifetimes before and after acceptor photobleaching. The graph contains data from different cell samples and two different donor–acceptor pairs. The observed changes are insignificant. (****$P <$ 0.0001, **$P = 0.0053$, not significant – ns: $P > 0.05$).

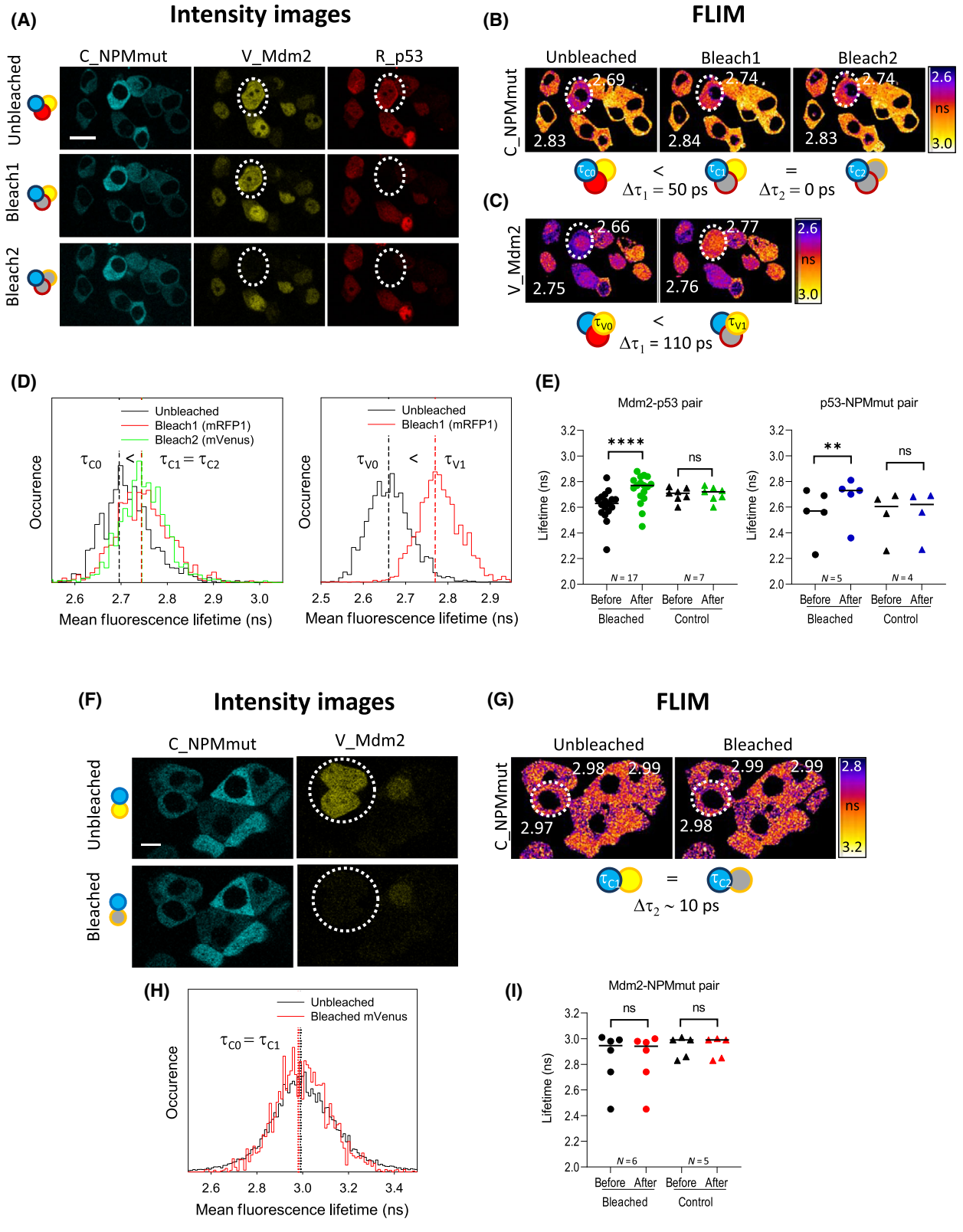

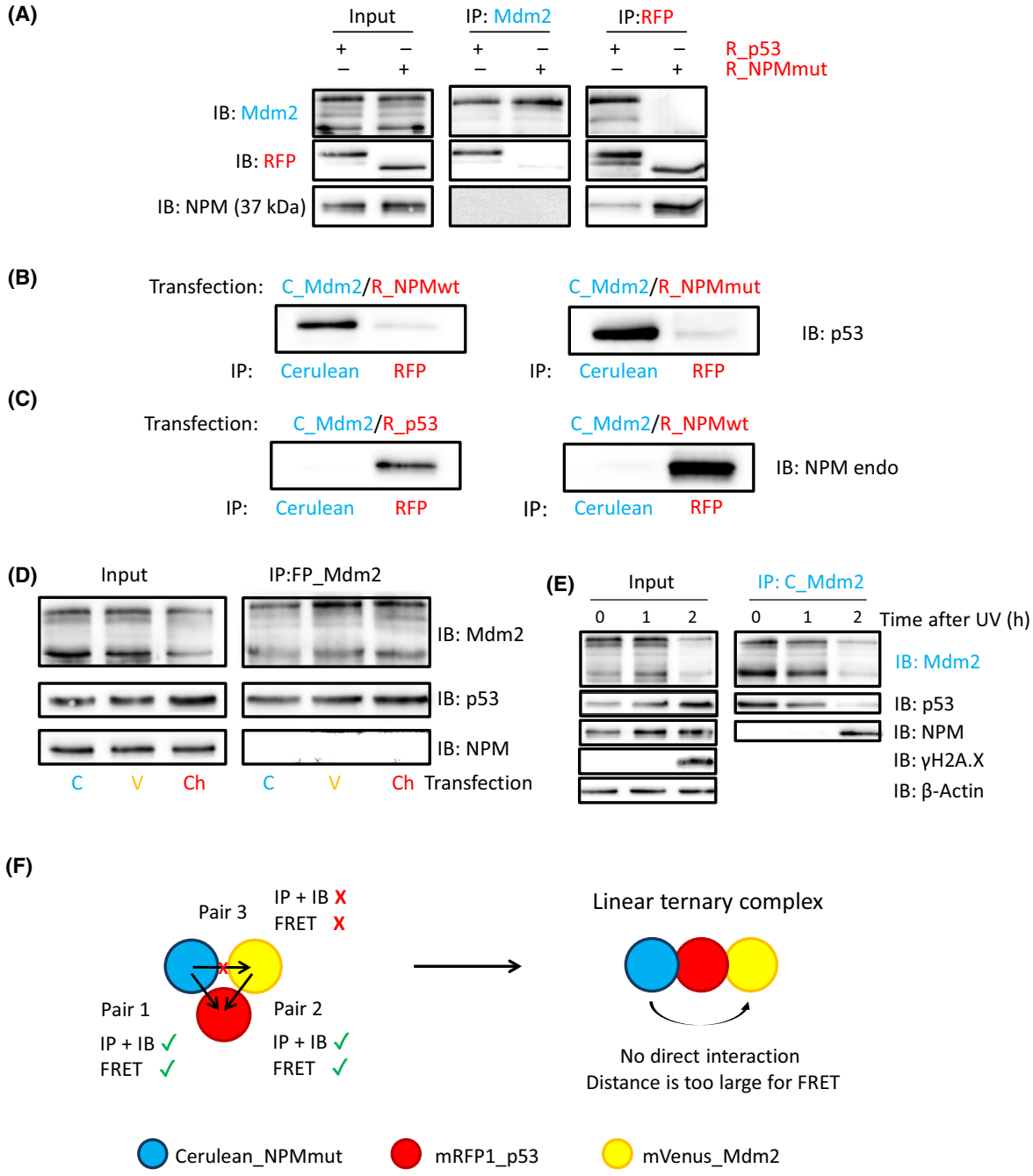

Fig. 4. Interaction of Mdm2, p53 and NPMwt/mut in lysates of double- and single-transfected HEK-293T cells. (A) Cells transfected with C_Mdm2 and cotransfected with R_p53 or R_NPMmut. Mdm2 interacts with p53 in all samples. Endogenous NPM co-precipitates with both R_p53 and R_NPMmut. Neither exogenous nor endogenous NPM co-precipitate with C_Mdm2 and, vice versa, C_Mdm2 does not co-precipitate R_NPMmut. Identical results were obtained with R_NPMwt (data not shown). (B) p53 co-precipitates with Mdm2 more than with NPM variants. (C) Endogenous NPM co-precipitates with p53 and NPMwt. It does not precipitate with Mdm2. (D) Single transfection with C_Mdm2 (C), V_Mdm2 (V) and mCherry_Mdm2 (Ch). Endogenous p53 co-precipitates with all variants of Mdm2. Endogenous NPM is not found in any precipitate. Cerulean- and mVenus-fused proteins were immunoprecipitated with GFP-Trap and mCherry-fused proteins with RFP-Trap. (E) Interaction of Mdm2 with NPM after UV irradiation. HEK-293T cells transfected with C_Mdm2 were UVC-irradiated (800 $J \cdot m^{-2}$ @ 254 nm) and lysed at indicated times. C_Mdm2 immunoprecipitation was performed and level of co-precipitated p53 and NPM was detected by WB. γH2A.X expression was evaluated to estimate the extent of DNA damage. (F) Scheme of the chain-like ternary complex based on the 3FF and immunoprecipitation experiments. Experiments were performed in triplicates.

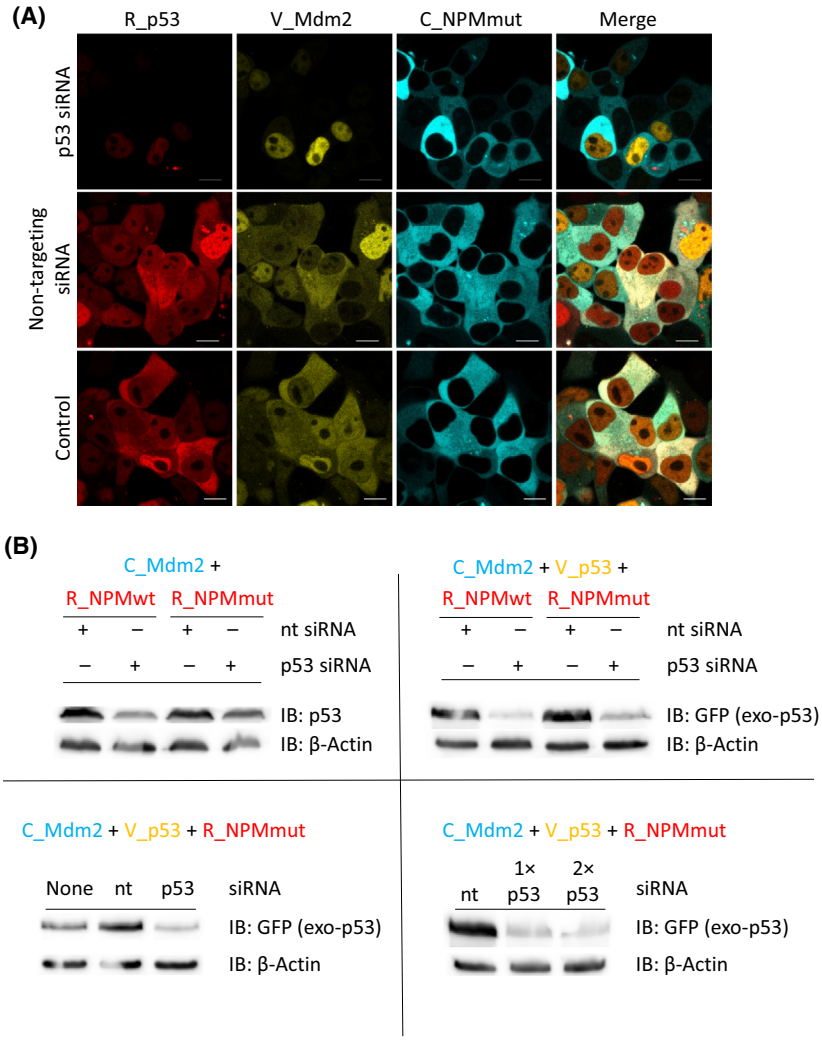

Fig. 5. p53 silencing. (A) Effect of p53 silencing on the cellular localization of V_Mdm2 and C_NPMmut in live HEK-293T cells. (1st row) – Cells transfected with p53-targeting siRNA. p53 is silenced, Mdm2 and NPMmut anti-colocalize in the nucleus and cytoplasm respectively. (2nd row) – Control cells transfected with non-targeting siRNA. NPMmut, p53 and Mdm2 colocalize in the cytoplasm. (3rd row) – Control cells without siRNA. Bar is 10 μm ($N = 5$). (B) Effect of p53 silencing on the p53 expression level. Upper left: level of endogenous p53 in C_Mdm2 and R_NPMwt/mut transfected cells with non-targeting (nt) and p53-targeting (p53) siRNA. Upper right: level of exogenous p53 in C_Mdm2, V_p53 and R_NPMwt/mut transfected cells with either non-targeting or p53-targeting siRNA. Lower left: level of exogenous p53 in C_Mdm2, V_p53 and R_NPMmut transfected cells with and without siRNA. Lower right: level of exogenous p53 in C_Mdm2, V_p53 and R_NPMwt/mut transfected cells in the presence of 50 nM (1×) and 100 nM (2×) siRNA concentrations. Exogenous p53 was detected with α-GFP antibody recognizing the Venus tag. β-Actin serves as a loading control, $N = 3$.

NPM interaction was found only in cells exposed to UV irradiation [27,28], where the delayed onset of the interaction is clearly seen (Fig. 4E). The figure also documents that the immunoprecipitation is sensitive enough to detect the interaction, if it is present.

In summary, we have unambiguously confirmed the Mdm2–p53 interaction, as well as interaction between p53 and both NPMmut and NPMwt variants. Localization experiments have shown explicit correlation between cytoplasmic localization of Mdm2 and the presence of NPMmut that is mislocalized to the cytoplasm due to the mutation introducing nuclear export signal [1]. All these evidences suggest NPMmut-induced cotransport of Mdm2 to the cytoplasm in some form of the NPMmut–p53–Mdm2 ternary complex. Nevertheless, despite all experimental efforts, we were unable to detect direct interaction between Mdm2 and NPM variants neither *in vivo* by FRET-FLIM nor in cell lysates by the immunochemical methods. The model of a compact "triangular" ternary complex schematically

depicted in Fig. 2 is, therefore, inconsistent with the experimental data, since it requires mutual interaction or close proximity of all three protein constituents. The direct interaction should be visible in the immunoprecipitation data, and the close proximity of Mdm2 and NPM should be detectable by FRET. Because none of the methods gave positive answer, we conclude that the NPMmut and Mdm2 separation is likely larger than the Cerulean-mRFP1 FRET pair can detect ($\sim$ 70 Å) [36,39]. Based on the results, it is legitimate to suggest that the cytoplasmic cotransport of Mdm2 and NPMmut is mediated by p53, which bridges NPMmut and Mdm2 in the chain-like NPMmut–p53–Mdm2 structure schematically depicted in Fig. 4F.

To challenge the above-outlined hypothesis, we silenced p53 in cells co-transfected with R_p53 V_Mdm2 and C_NPMmut (Fig. 5). Typical protein localization images of the p53-silenced cells and two different control samples are shown in Fig. 5A. We can see that p53-targeting siRNA causes uncoupling of V_Mdm2 from C_NPMmut. As a result, Mdm2 remains in the nucleus while NPMmut is exported to the cytoplasm. Without silencing, all three proteins colocalize in the cytoplasm of both control samples. Figure 5B demonstrates reduced levels of both endogenous and exogenous p53 after its silencing by targeting siRNA. The residual p53 expression was not inhibited even with using a higher siRNA concentration (lower right panel in Fig. 5B). The suppressed p53 levels can be detected both in cells with and without NPMmut. Altogether, results in Fig. 5 strongly point to p53 being a linker in the NPMmut–p53–Mdm2 complex.

Nutlin-3A breaks the NPMmut–p53–Mdm2 chain

Nutlin-3A is supposed to disrupt or compromise interaction between Mdm2 and p53 by blocking the main binding site for p53 on Mdm2 [8,9]. In this case, Nutlin-3A is also expected to disrupt the NPMmut–p53–Mdm2 complex similar to p53 silencing. As a consequence, Mdm2 should shuttle back to its regular nuclear location [40], not being exported by NPMmut–p53 complex. First, we examined the effect of Nutlin-3A on lysates of cells co-transfected with V_Mdm2 and R_p53. Immunoblots from immunoprecipitation in Fig. 6 document that within 2 h after its addition Nutlin-3A weakens the Mdm2–p53 interaction. The residual interaction sustains for at least 24 h. The full inhibition was not observed, which is consistent with a reported secondary binding site for p53 in the acidic domain of Mdm2 [9]. The interaction between p53 and NPM seems not to be significantly affected. Next, we tested the effect of Nutlin-3A in live cells by the 3FF. As seen in Fig. 7A, V_Mdm2 relocalizes from the cytoplasm back to the nucleus. The relocalization is clearly observable in 25 min and highly progresses in 85 min after the Nutlin-3A addition. The relocalization is accompanied by gradual increase of the V_Mdm2 fluorescence lifetime in the nucleus (Fig. 7B). This implies separation of V_Mdm2 and R_p53 and weakening of FRET between them. Importantly, both C_NPMmut and R_p53 stay localized in the cytoplasm. The results further support our hypothesis that the presence of Mdm2 in the cytoplasm of NPMmut-containing cells depends on its interaction with delocalized p53 (Fig. 7D).

The relocalization seems to be finished within 2 h, as documented by the time evolution of the intensities in the nucleus and the cytoplasm in Fig. 7E. The time scale of the process is consistent with the immunoprecipitation data in Fig. 6. We conclude that several lines of experimental evidence speak for the chain-like model of the NPMmut–p53–Mdm2 complex, where p53 is a crucial central-bridging element.

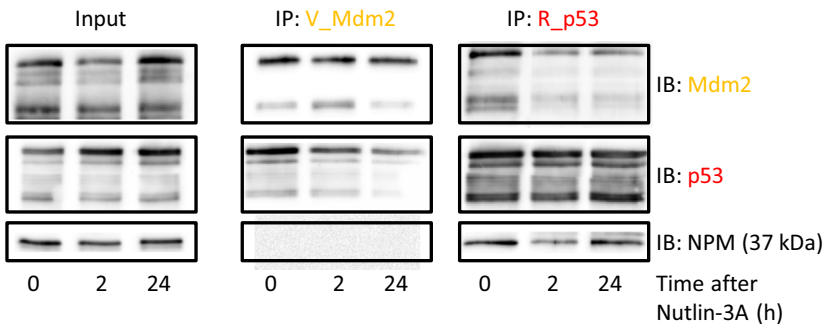

Fig. 6. Mdm2–p53 interaction in lysates of HEK-293T cells cotransfected with mVenus_Mdm2 (V_Mdm2) and mRFP1_p53 (R_p53). The cell lysis and immunoprecipitation were done at 0, 2 and 24 h after the addition of 10 μM Nutlin-3A to the live cell culture. It is seen that Nutlin-3A weakens the Mdm2-p53 interaction within 2 hours after the addition, full inhibition of the Mdm2–p53 interaction is not observed. Experiments were performed in triplicates.

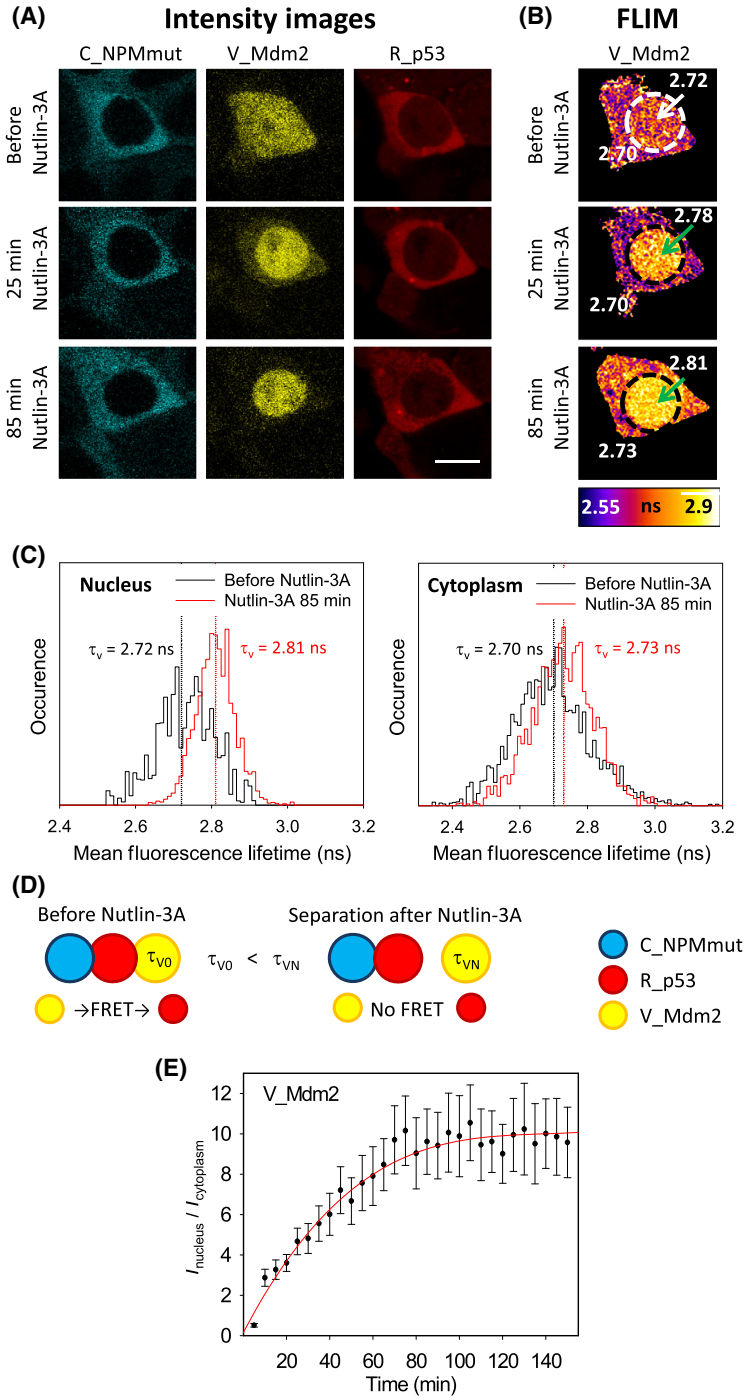

Fig. 7. Effect of Nutlin-3A on the Mdm2–p53 interaction in HEK-293T cells cotransfected with C_NPMmut, V_Mdm2 and R_p53. (A) Columns from left to right are fluorescence intensities of C_NPMmut, V_Mdm2 and R_p53. Rows represent situation before and after the addition of 10 μM Nutlin-3A. (B) Fluorescence lifetime images of V_Mdm2 before and after addition of Nutlin-3A. Mean lifetime values in the cytoplasm and in the nucleus are indicated in the images. (C) Fluorescence lifetime distributions corresponding to the panel B ($N = 5$ for A, B). (D) Disruption of the NPMmut–p53–Mdm2 complex by Nutlin-3A. Coloured circles represent protein tagging. Disruption of the Mdm2–p53 interaction is evaluated from the increase in the C_Mdm2 fluorescence lifetime upon the Nutlin-3A addition. (E) Time dependence of the ratio of emission intensities in the nucleus and in the cytoplasm averaged over the ensemble of Nutlin-3A-treated cells ($N = 10$). Error bars represent 95% confidence limit of the average and reflect variation in the cell response to the Nutlin-3A treatment. The red line serves merely as a guide for the eye. Bar is 10 μm.

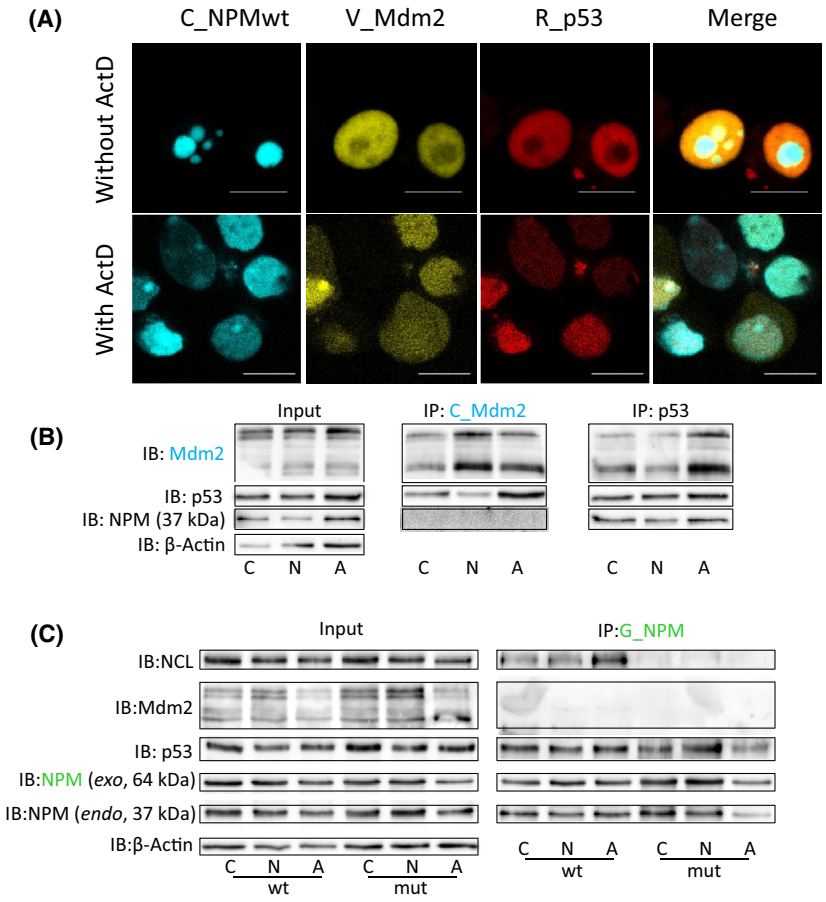

Fig. 8. Effect of Actinomycin D and Nutlin-3A on the Mdm2–p53 interaction in HEK-293T cells. (A) Localization of C_NPMwt, V_Mdm2 and R_p53 in live HEK-293T cells in the presence of ActD. (1st row) – Cells without ActD, (2nd row) – cells treated with 10 nM ActD for 24 h. Better colocalization of NPMwt and Mdm2 is clearly visible in the presence of ActD. Bar is 10 μm. (B, C) Immunoprecipitation of Cerulean/GFP by GFP-Trap. (B) Single transfection with C_Mdm2. Nutlin-3A attenuates Mdm2–p53 interaction, NPM does not precipitate with Mdm2 in any sample. Lane legend: C – control, *N* – 10 μM Nutlin-3A, A – 10 nM ActD. (C) Single transfection with eGFP-tagged NPM variants, G_NPM (wt/mut). NPM–p53 interaction is unaffected by Nutlin-3A (lane legends same as in B). Experiments were performed in triplicates.

Interactions in the NPMmut–p53–Mdm2 complex are not affected by Actinomycin D

UV radiation was reported to induce transient NPM/Mdm2 interaction [27,28] mediated by SIRT7-driven NPM acetylation [28]. We, therefore, tested, whether the AML-relevant genotoxic drug ActD [41,42], which upregulates both p53 and Mdm2 [6,43] without SIRT7 amplification [28], can affect interactions within the complex. Despite upregulated Mdm2 and its better colocalization with NPM in the nucleoplasm (Fig. 8A), we did not detect any interaction between Mdm2 and NPM variants (Fig. 8B,C). It has to be mentioned that we were able to reproduce and detect the UV-induced interaction of NPM with Mdm2, which proves that the interaction is detectable (Fig. 4E). Interaction of Mdm2 and NPMwt/mut with p53 persisted in ActD-treated cells (Fig. 8B,C). The presence of p53 in NPM-precipitates of Nutlin-3A-treated cells fully agrees with the localization results (Fig. 7A) and demonstrates persisting p53–NPM interaction in the presence of Nutlin-3A (Fig. 8C). According to previous findings [44], loss of NPM interaction with nucleolin (NCL) due to the NPM mutation remained unaffected after the Nutlin-3A or ActD treatment (Fig. 8C).

Endogenous proteins in AML cell lines behave similar to fluorescently labelled proteins in HEK-293T model system

To validate our results in relevant system, we evaluated Mdm2–p53–NPM interactions in AML cell lines. Due to very low concentrations of p53 and Mdm2 in

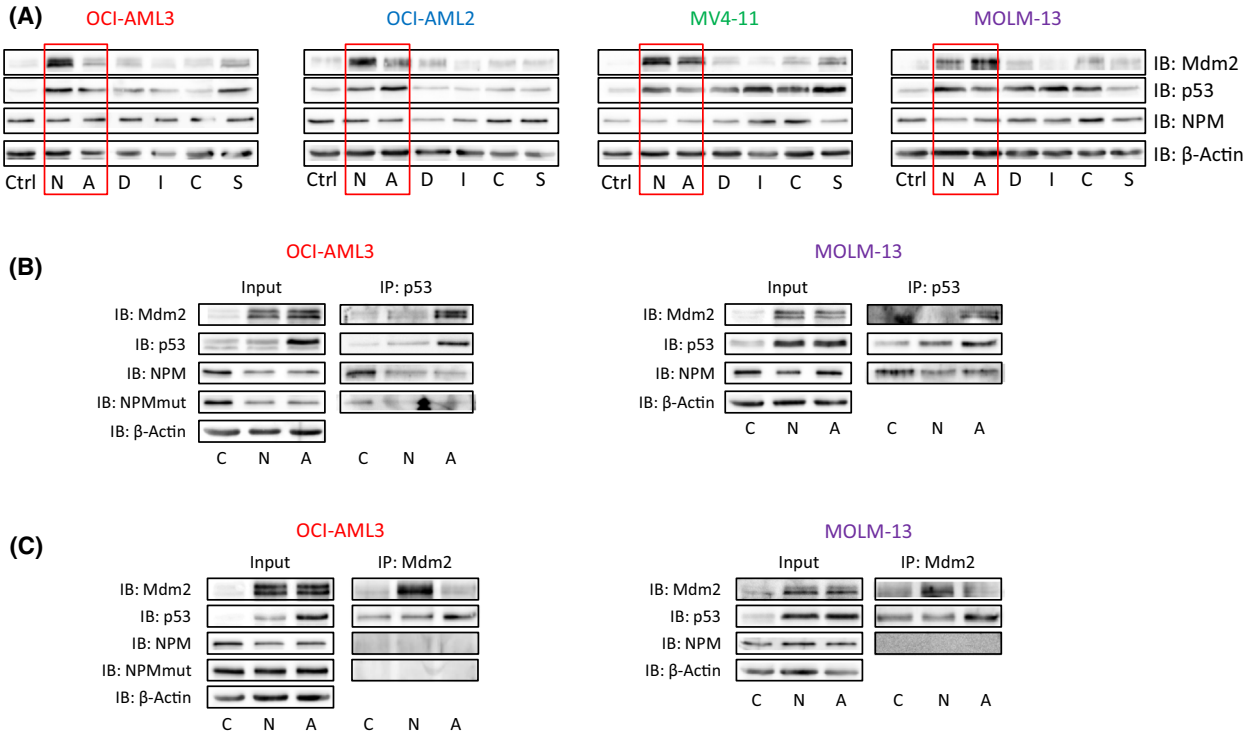

Fig. 9. Effect of cytostatics in AML cell lines. (A) Mdm2, p53 and NPM expression after 24-h treatment with cytostatics. Ctrl – Untreated control, *N* – 5 μM Nutlin-3A, A – 2 nM ActD, D – 1 μM doxorubicin, I – 200 Nm idarubicin, C – 5 μM Cytarabine, S – 0.5 μM Selinexor. Level of β-actin served as a loading control ($N=3$). (B, C) Effect of Nutlin-3A and ActD on the Mdm2–p53–NPM interaction complex in OCI-AML3 (with NPMmut) and MOLM-13 (NPMwt only) cell lines respectively. (B) p53 immunoprecipitation ($N=4$), (C) Mdm2 immunoprecipitation ($N=2$).

intact cells, we first searched for conditions inducing detectable levels of these two proteins. As seen in Fig. 9, screening of clinically relevant cytotoxic drugs revealed only Nutlin-3A and ActD to systematically increase p53 and Mdm2 levels in our panel of AML cell lines. ActD-treated cells, therefore, represented positive control in subsequent p53- and Mdm2-immunoprecipitation experiments. Results from the AML cell line with NPM mutation (OCI-AML3) and from the line containing wild-type NPM only (MOLM-13) are presented in Fig. 9B,C. Similar to HEK-293T cells, evaluation of co-immunoprecipitated Mdm2 in p53 immunoprecipitates confirmed weakening of the Mdm2–p53 interaction in Nutlin-3A-treated samples (Fig. 9B). Decreased NPM level in Nutlin-3A and ActD-treated samples, likely induced by a lower demand on the ribosome synthesis, is also mirrored in p53 precipitates. Similarly, Mdm2 immunoprecipitates also contained less p53 in the samples treated with Nutlin-3A (Fig. 9C). Despite the increased Mdm2 levels, NPM was not found in Mdm2 immunoprecipitates. This fully supports conclusions made with fluorescently labelled proteins in HEK-293T cells.

Discussion

Several research groups searched for the interaction between NPM and Mdm2 with ambiguous results. While Bertwistle *et al.* [45] did not find the interaction and claimed its existence unlikely, others [10,28] found NPM in Mdm2 precipitates of cancer cells treated by UV light or proteasome inhibitor MG132 [46]. The *in vitro* NPM–Mdm2 interaction was reported to be modulated by amount of *in vitro*-translated p53 added to the suspension [10].

We have recently shown that the AML-associated NPM mutation causes aberrant p53 localization [5]. Here, we document that NPMmut affects also the cellular localization of Mdm2. The presence of Mdm2 in the cytoplasm is strongly NPMmut dependent, i.e., it was not observed in cells transfected with NPMwt instead of NPMmut. Our results imply that NPM mutation plays an important role in the regulation of the NPM–p53–Mdm2 interaction network with high relevance to AML pathogenesis.

FRET-FLIM and immunoprecipitation experiments have previously proved that the behaviour of

fluorescently labelled exogenous NPM and p53 well describes interaction between the endogenous protein forms in live cells [5]. In this work, we performed experiments with a triad of tagged model proteins in order to establish a platform for detection of ternary complexes by 3FF measurements. Highly oligomerizing NPMwt and NPMmut variants [7,37,38] were fused to Cerulean, mVenus and mRFP1, produced in live cells and utilized for detection of the ternary complexes. The experiments proved that the choice of fluorophores constitutes a suitable set of donor–acceptor pairs for 3FF measurements. In order to match emission characteristics and FRET efficiencies of the fluorophores with different expression levels of NPM, p53 and Mdm2, we performed permutations of the fluorescent tagging. The procedure yielded an optimal labelling scheme further used for the 3FF experiments.

Despite our localization experiments clearly revealed tight correlation between expression of NPMmut and the cytoplasmic localization of both Mdm2 and p53 in transfected cells, we were unable to detect interaction between Mdm2 and NPMmut that could explain the protein cotransport to the cytoplasm. Neither labelled nor endogenous NPMwt was found to interact with Mdm2 in intact cells. The absence of NPMmut–Mdm2 interaction is, thus, not related to the NPM mutation. Nevertheless, we clearly detected the interaction between the p53–NPMmut and the p53–Mdm2 protein pairs. We, therefore, suggest that Mdm2–p53–NPMmut complex adopts a chain-like structure, which facilitates the observed cotransport of Mdm2 from the nucleus to the cytoplasm together with NPMmut. p53 serves as a bridging element there and mediates formation of such complex (Fig. 4F). We cannot predict geometry of the complex more accurately from our experiments. Nevertheless, the absence of FRET between Cerulean and mVenus with the critical Förster distance of $R_0 \sim 55$ Å [39] suggests separation of the donor and acceptor larger than about $2R_0$, i.e., ~ 100 Å [36].

The p53 protein has an intrinsically flexible structure [47], which self-associates to structurally plastic oligomers [48]. Based on *in vitro* measurements of the K_d [49] and p53 basal concentration in cells [50], it was suggested that p53 assumes predominantly dimeric structure under normal conditions [49,50]. However, recent *in vivo* experiments revealed a broader oligomer representation, p53 being distributed among significant populations of monomers, dimers and tetramers. The equilibrium between the states is regulated by protein–protein interactions [51]. We do not know, which oligomeric state is bound in the suggested Mdm2–p53–NPMmut complex. Nevertheless, monomeric p53 (p53L344P mutant) displayed reduced ability to bind Mdm2 [52]. On the contrary, tetramerization was shown to be important for p53 to bind Mdm2, since the loss of the quaternary structure severely impaired the p53 binding [53]. Interacting regions between dimeric p53 and Mdm2 have also been found [54]. We, therefore, speculate that the Mdm2–p53–NPMmut complex should likely accommodate tetrameric or dimeric p53. The shape of tetrameric p53 (Mw $\sim$ 180 kDa [55]) is a skewed cube of 66 Å × 82 Å × 85 Å in size. Its overall volume corresponds to a 400 kDa globular protein [48]. The p53 dimer would be similarly bulky. We assume that such "spacer" between Cerulean_NPMmut and mVenus_Mdm2 easily prevents FRET between those molecules (Fig. 4F).

To verify the proposed model, we targeted p53 with siRNA and indeed, p53 silencing led to the exclusively nuclear localization of Mdm2 in the presence of NPMmut. Further, we investigated disruption of Mdm2–p53 interaction by Nutlin-3A. Substantial weakening of the Mdm2–p53 interaction was observed in precipitates of Nutlin-3A-treated cells. Nevertheless, the interaction partially persisted regardless of the treatment duration. This is in full agreement with reported multiple binding sites of Mdm2 for the p53 molecule [8]. Interaction of p53 with NPM remains almost unaffected [32]. Importantly, in the live-cell experiments, Nutlin-3A caused significant relocalization of V_Mdm2 to the nucleus, while R_p53 and C_NPMmut stayed in the cytoplasm (Fig. 7). The relocalization was accompanied by the loss of FRET between V_Mdm2 and R_p53 after the release of Mdm2 from the NPMmut–p53–Mdm2 complex. All these results strongly support our hypothesis of Mdm2 being driven into the cytoplasm of NPMmut-expressing cells by its tight association with p53.

The NPM–Mdm2 interaction was previously found under genotoxic conditions. Specifically, under UV-induced stress, NPM is transiently bound to Mdm2 causing a release of p53 from its interaction with Mdm2 and also increase in p53 activity and stability [27–29]. Due to the ability to induce genotoxic stress, we expected similar effect with DNA-damaging ActD, which has a potential for AML treatment, too [41]. Nevertheless, ActD did not induce interaction between Mdm2 and any variant of NPM. The UV-induced NPM–Mdm2 interaction was reportedly associated with SIRT7-mediated NPM acetylation, which was not detected after the ActD treatment [28]. As concerns the participation of NPM, we speculate that mechanisms of the DNA-damage repair likely differ in ActD- and UV-treated cells.

Immunoprecipitation experiments with AML cell lines proved partial inhibition of the Mdm2–p53

interaction by Nutlin-3A and the absence of the interaction between NPM and Mdm2. These results obtained on a relevant system of endogenous proteins confirmed our findings from HEK-293T cells.

In conclusion, we have shown that in the context of AML, the cytoplasmic mislocalization of Mdm2 associated with the presence of NPMmut is mediated by p53. Several lines of evidence witness the existence of the chain-like NPMmut–p53-Mdm2 complex, where p53 constitutes a central-bridging element. There are no signs of direct NPM–Mdm2 interaction under the native conditions. The stability of the complex is compromised in the presence of Nutlin-3A, which causes partial inhibition of the Mdm2–p53 interaction and results in Mdm2 nuclear relocalization and p53 stabilization. This could certainly contribute to the restoration of regulatory functions in cells with NPMmut.

Materials and methods

Cell cultivation

Adherent cell line HEK-293T was kindly provided by Š. Němečková (Department of Immunology, Institute of Hematology and Blood Transfusion). Leukaemia cell lines OCI-AML2, OCI-AML3, MV4-11 and MOLM-13 were obtained from DSMZ (Braunschweig, Germany). The cells were cultivated according to the manufacturer's recommendations. Specifically, HEK-293T were cultivated in DMEM growth media (Merck, Darmstadt, Germany) with 10% FBS (Biosera, Cholet, France) and antibiotics (100 $U \cdot mL^{-1}$ penicillin, 100 $\mu g \cdot mL^{-1}$ streptomycin; Merck). OCI-AML2 and OCI-AML3 grew in α-MEM (Merck) supplemented with 20% FBS, L-glutamine (Merck) and antibiotics. MV4-11 and MOLM-13 were cultivated in RPMI-1640, with 10% FBS, L-glutamine and antibiotics. Nutlin-3A (Selleckchem, Planegg, Germany) and Actinomycin D (Merck) were injected into the cell culture from the 10 mM and 10 μM stock solution, respectively, to the final concentrations specified in the text.

For UV treatment, cells were exposed to 800 $J \cdot m^{-2}$ of UVC, 254 nm (Crosslinker ULTRA-LUM Inc., Claremont, CA, USA). The medium was taken away prior to the irradiation to re-supplement the cells afterwards. Then, the cells were incubated for 1 or 2 h at 37 °C (5% CO_2) and analysed subsequently.

Plasmid construction and cell transfection

Plasmids for expression of fluorescently tagged proteins were constructed by standard techniques of molecular cloning. Construction of plasmids for expression of NPM variants (NPMwt and NPMmut) fused with mRFP1 was described in Ref. [6] and for expression of p53 fused with mRFP1 in [5]. For cloning Cerulean-labelled NPM variants, DNA fragments corresponding to the NPM variants were excised by XhoI and BamHI restrictases (Thermo Scientific, Waltham, MA, USA) from the plasmids expressing mRFP1-fusion constructs. Then, they were ligated into vector Cerulean-C1 (Plasmid #54604; Addgene [56]) with T4 DNA ligase (NEB) using XhoI and BamHI unique restriction sites. The Cerulean-C1 plasmid was a gift from Davidson and Piston [57]. Sequence for Cerulean was replaced in these plasmids with mVenus to prepare plasmids for mVenus-tagged expression. In detail, DNA fragments of mVenus were PCR-amplified from mVenus N1 (Plasmid #27793; Addgene [58]) using extended primers containing XbaI and XhoI (Thermo Scientific) restriction sites. The fragments were then subcloned to the plasmids for tagging with Cerulean, where Cerulean sequence was excised with NheI and XhoI restriction enzymes (Thermo Scientific). The mVenus N1 plasmid was a gift from Vogel [59]. For cloning *MDM2* containing constructs, DNA fragments corresponding to specific *MDM2* transcript isoform (RefSeq. NM_002392.6 from NCBI database) were PCR-amplified from plasmid MDM2p-Mdm2-YFP (Plasmid # 53962; Addgene [60]) using extended primers and subsequently they were subcloned to vectors Cerulean-N1 and mVenus N1 (Plasmids #54742 and #27793, respectively; Addgene [56,58]) using unique sites for XhoI and BamHI restrictases (Thermo Scientific) and T4 DNA ligase (NEB). The MDM2p-Mdm2-YFP plasmid was a gift from Alon and Lahav [61]. The Cerulean-N1 was a gift from Davidson and Piston [62].

The constructed plasmids were amplified in *Escherichia coli* competent cells and purified with the PureYield Plasmid Miniprep System (Promega, Madison, WI, USA). Twenty-four hours prior to transfection, HEK-293T cells were seeded to the cell density of 1×10^5 mL^{-1} and then transfected with jetPrime transfection reagent (Polyplus Transfection, Illkirch-Graffenstaden, France) according to the manufacturer's protocol. Growth medium was replaced 4 h after the transfection and cells were further grown for 20–40 h prior to analysis. All protein constructs except Mdm2 ones were tagged on their N terminus.

ON-TARGETplus siRNA (Dharmacon, Lafayette, CO, USA) targeting TP53 (#L-003329) was used for silencing the *TP53* expression. Non-targeting siRNA (#D-001810) served as the control. siRNAs were co-transfected together with appropriate DNA plasmids using the jetPRIME transfection reagent (Polyplus Transfection) according to the manufacturer's instructions. The siRNA concentration ranged from 50 nM to 100 nM (final concentration in the jetPRIME buffer prior to transfection). The growth medium was replaced 24 h after the transfection and cells were further grown for 20–40 h prior to measurement.

Live-cell imaging

Cells were grown on glass bottom Petri dish (Cellvis, Mountain View, CA, USA). Fluorescence experiments were

carried out at 37 °C after sealing the Petri dish with parafilm to prevent CO_2 leakage. The subcellular distribution and co-localization of FP-fused protein variants were observed under the confocal laser scanning microscope FV1000 (Olympus Corporation, Hamburg, Germany) with UPLSAPO 60× NA 1.35 oil immersion objective (Olympus). If not specified differently, a Petri dish was typically imaged for 1 h and data were processed by the FluoView FV10-ASW 3.1. Cerulean, mVenus and mRFP1 emission was sequentially excited at 405, 488 and 543 nm, respectively, using DM405/488/543/647 at the excitation path. For the detection of Cerulean, emitted light was collected with BA430-490 bandpass filter. For mVenus and mRFP1 detection, the emitted light passed through FV12-MHBY filter cube and was detected with high sensitivity GaAsP detectors (Olympus). All live-cell imaging including FLIM experiments were done in several multiplicates, typically on different days with different cell cultures.

FLIM – data acquisition and analysis

Fluorescence lifetime imaging was performed on the apparatus described previously [63]. Briefly, FLIM was carried out on the inverted IX83 microscope with FV1200 confocal scanner (Olympus). The microscope was equipped with cell-cultivation chamber (Okolab, Naples, Italy) and FLIM add-on comprising picosecond semiconductor lasers, GaAsP hybrid detectors and TimeHarp 260PICO TCSPC detection electronics (all PicoQuant, Berlin, Germany). Cellular FLIM experiments were performed with the UPLSAPO 60× NA 1.2 water immersion objective (Olympus). Cerulean fluorescence was excited at 405 nm by the picosecond LDH-DC-405 laser (PicoQuant) with the dual-band 405/488 dichroic in the excitation path and the Semrock 470/24 bandpass filter in the detection channel. mVenus fluorescence was excited at 485 nm by the picosecond LDH-DC-485 laser (PicoQuant) with the dual-band 405/488 dichroic in the excitation path and the Semrock 534/30 bandpass filter in the detection path. To avoid pile-up, the data collection rate at the brightest pixels was kept below 5% of the laser repetition rate, which was kept at 20 MHz. mVenus and mRFP1 photobleaching of selected ROIs was done by the 514.5 nm and 562 nm cw laser respectively (Olympus).

Fluorescence lifetime imaging data were analysed using the SYMPHOTIME64 software (PicoQuant). The lifetime images were generated in the SYMPHOTIME64 by the "fast-FLIM" approach when mean pixel lifetimes were calculated by a method of moments [48]. Specifically, the lifetime τ_{fast} was determined as the difference between the barycentre of the fluorescence decay and the time-offset t_{offset} at the steepest growth of the decay curve at each pixel:

$$\tau_{fast} = \frac{\sum I_i t_i}{\sum I_i} - t_{offset}, \quad (1)$$

where I_i stands for the emission intensity at time t_i. A least-squares reconvolution was applied for accurate analysis of cumulative decays from ROIs (e.g. cell, nucleus and nucleolus). Emission of fluorescence proteins was typically assumed to decay bi-exponentially according to the following formula:

$$I(t) = a_1 \cdot e^{-t/\tau_1} + a_2 \cdot e^{-t/\tau_2}, \quad (2)$$

where τ_i and a_i are lifetime components and corresponding amplitudes respectively. The intensity-weighted mean fluorescence lifetime was calculated as:

$$\tau_{mean} = \sum f_i \cdot \tau_i, f_i = a_i \tau_i / \sum a_i \tau_i, \quad (3)$$

where f_i are intensity fractions of the i-th lifetime component. Standard deviations of τ_{mean} were determined by the statistical bootstrap method [64] and were always lower than ±0.02 ns.

Immunofluorescence

Cells transfected with Cerulean_NPMmut and mVenus_Mdm2 were fixed with 4% paraformaldehyde and permeabilized with 0.5% Triton-X100. Then, the samples were sequentially incubated with mouse monoclonal anti-p53 antibody (Santa Cruz Biotechnology, Dallas, TX, USA) and anti-mouse AlexaFluor555-conjugated secondary antibody (ThermoFisher Scientific). Immunofluorescence was collected together with Cerulean and mVenus fluorescence similarly as for Live Cell Imaging.

Co-immunoprecipitation and trap assay

Transfected cells expressing FPs were processed after 40-h incubation. GFP-, RFP- and p53-Trap_A system (Proteintech, Planegg-Martinsried, Germany) were used following the manufacturer's instructions as described in Ref. [31]. Due to the structural similarity of Cerulean, mVenus and GFP, the GFP-Trap system was used for precipitation of both Cerulean and mVenus. mRFP1- and mCherry-labelled proteins were precipitated by the RFP-Trap. The p53-Trap system was used for precipitation of endogenous p53 from cells untransfected with fluorescently-labelled p53. Briefly, FP-expressing adherent cells were washed with ice-cold PBS and scrapped from dish. The cell pellet was lysed in the lysis buffer (10 mM Tris/Cl pH 7.5, 150 mM NaCl, 0.5 mM EDTA, 0.5% NP-40, protease and phosphatase inhibitors) on ice for 30 min and centrifuged at 20 000 *g* / 10 min / 4 °C. The lysate was applied to the Trap_A beads and rotated for 1 h at 4 °C. Then, the beads were pelleted and extensively washed in the diluting buffer (10 mM Tris/Cl pH 7.5, 150 mM NaCl, 0.5 mM EDTA), resuspended in 2×SDS sample buffer (100 mM Tris pH 6.8, 4% SDS, 200 mM DTT, 20% glycerol), boiled for 10 min and centrifuged

at 2500 *g* / 2 min / 4 °C. Supernatant was stored at -20 °C until used for SDS/PAGE. We performed at least three replicates per experiment.

For precipitation of the p53 from lysates of leukaemia cell lines, the protocol was identical as for the endogenous p53-Trap from adherent cells (see above). To precipitate the Mdm2, we mixed cell lysate with rabbit monoclonal anti-Mdm2 antibody (Abcam, Cambridge, UK) and the mixture was rotated for 2 h/4 °C. Then, A/G-agarose beads (Santa Cruz Biotechnology) were added, the samples were rotated for additional 1 h/4 °C and immunoprecipitates were handled identically as in the Trap protocol.

Western blotting

Five to ten microliters of each sample were subjected to SDS/PAGE and transferred into PVDF membrane (BioRad, Hercules, CA, USA). Mouse monoclonal antibodies against β-Actin, p53, dsRed, GFP, NCL and NPM (clone 3F291, for endogenous NPM), were from Santa Cruz Biotechnology. All mouse primary antibodies were used at a dilution of 1 : 100–1 : 500. Rabbit monoclonal antibodies against Mdm2 and H2A.X phosphorylated at Ser139 (γH2A.X; Abcam) were used at 1 : 1000 dilution. Anti-mouse and anti-rabbit HRP-conjugated secondary antibodies were purchased from Thermo Scientific and used at concentrations 1 : 10 000–1 : 50 000. ECL Plus Western Blotting Detection System (GE Healthcare, Chicago, IL, USA) was used for chemiluminescence visualization and evaluation by G-box iChemi XT4 digital imaging device (Syngene Europe, Cambridge, UK). Alternatively, SuperSignal West Atto Ultimate Sensitivity Substrate (ThermoFisher Scientific) was used for highly sensitive detection of co-immunoprecipitated proteins. Images included in Figures are always representative of at least three independent experiments.

Acknowledgements

The work was supported by the Czech Science Foundation – grant No 22-03875S. BB acknowledges the support of the Ministry of Health of the Czech Republic – project for conceptual development of the research organization (No. 00023736).

Conflict of interest

The authors declare no conflict of interest.

Author contributions

PH and BB conceived the research and provided scientific guidance; AH constructed plasmids and transfected cells; BB and KW performed immunoprecipitation and western blot analysis; DS, AH, BB and PH made imaging and FLIM experiments; DS analysed the FRET-FLIM data; PH and BB wrote the paper; all co-authors revised the manuscript.

Data availability statement

All data needed to evaluate the conclusions of this study are present in the article. Additional supporting data are available from corresponding authors upon reasonable request.

References

1 Falini B, Mecucci C, Tiacci E, Alcalay M, Rosati R, Pasqualucci L, La Starza R, Diverio D, Colombo E, Santucci A *et al.* (2005) Cytoplasmic nucleophosmin in acute myelogenous leukemia with a normal karyotype. *N Engl J Med* **352**, 254–266.

2 Arber DA, Orazi A, Hasserjian R, Thiele J, Borowitz MJ, Le Beau MM, Bloomfield CD, Cazzola M & Vardiman JW (2016) The 2016 revision to the World Health Organization classification of myeloid neoplasms and acute leukemia. *Blood* **127**, 2391–2405.

3 Brodska B, Sasinkova M & Kuzelova K (2019) Nucleophosmin in leukemia: consequences of anchor loss. *Int J Biochem Cell Biol* **111**, 52–62.

4 Bolli N, De Marco MF, Martelli MP, Bigerna B, Pucciarini A, Rossi R, Mannucci R, Manes N, Pettirossi V, Pileri SA *et al.* (2009) A dose-dependent tug of war involving the NPM1 leukaemic mutant, nucleophosmin, and ARF. *Leukemia* **23**, 501–509.

5 Holoubek A, Strachotova D, Otevrelova P, Roselova P, Herman P & Brodska B (2021) AML-related NPM mutations drive p53 delocalization into the cytoplasm with possible impact on p53-dependent stress response. *Cancers (Basel)* **13**, 3266.

6 Brodska B, Holoubek A, Otevrelova P & Kuzelova K (2016) Low-dose actinomycin-D induces redistribution of wild-type and mutated nucleophosmin followed by cell death in leukemic cells. *J Cell Biochem* **117**, 1319–1329.

7 Sasinkova M, Herman P, Holoubek A, Strachotova D, Otevrelova P, Grebenova D, Kuzelova K & Brodska B (2021) NSC348884 cytotoxicity is not mediated by inhibition of nucleophosmin oligomerization. *Sci Rep* **11**, 1084.

8 Yu GW, Rudiger S, Veprintsev D, Freund S, Fernandez-Fernandez MR & Fersht AR (2006) The central region of HDM2 provides a second binding site for p53. *Proc Natl Acad Sci USA* **103**, 1227–1232.

9 Ma JH, Martin JD, Zhang H, Auger KR, Ho TF, Kirkpatrick RB, Grooms MH, Johanson KO, Tummino PJ, Copeland RA *et al.* (2006) A second p53

binding site in the central domain of mdm2 is essential for p53 ubiquitination. *Biochemistry* **45**, 9238–9245.
10 Kurki S, Peltonen K, Latonen L, Kiviharju TM, Ojala PM, Meek D & Laiho M (2004) Nucleolar protein NPM interacts with HDM2 and protects tumor suppressor protein p53 from HDM2-mediated degradation. *Cancer Cell* **5**, 465–475.
11 Colombo E, Marine JC, Danovi D, Falini B & Pelicci PG (2002) Nucleophosmin regulates the stability and transcriptional activity of p53. *Nat Cell Biol* **4**, 529–533.
12 Li MY, Brooks CL, Wu-Baer F, Chen DL, Baer R & Gu W (2003) Mono-versus polyubiquitination: differential control of p53 fate by Mdm2. *Science* **302**, 1972–1975.
13 Brooks CL, Li MY & Gu W (2004) Monoubiquitination – the signal for p53 nuclear export? *Cell Cycle* **3**, 436–438.
14 Henningsen KM, Manzini V, Magerhans A, Gerber S & Dobbelstein M (2022) MDM2-driven ubiquitination rapidly removes p53 from its cognate promoters. *Biomolecules* **12**, 22.
15 Oliner JD, Pietenpol JA, Thiagalingam S, Gvuris J, Kinzler KW & Vogelstein B (1993) Oncoprotein Mdm2 conceals the activation domain of tumor suppressor-P53. *Nature* **362**, 857–860.
16 Kubbutat MHG, Ludwig RL, Ashcroft M & Vousden KH (1998) Regulation of Mdm2-directed degradation by the C terminus of p53. *Mol Cell Biol* **18**, 5690–5698.
17 Moll UM & Petrenko O (2003) The MDM2-p53 interaction. *Mol Cancer Res* **1**, 1001–1008.
18 Wallace M, Worrall E, Pettersson S, Hupp TR & Ball KL (2006) Dual-site regulation of MDM2 E3-ubiquitin ligase activity. *Mol Cell* **23**, 251–263.
19 Kalousek I, Brodska B, Otevrelova P & Roselova P (2007) Actinomycin D upregulates proapoptotic protein Puma and downregulates Bcl-2 mRNA in normal peripheral blood lymphocytes. *AntiCancer Drugs* **18**, 763–772.
20 Levine AJ (2019) The many faces of p53: something for everyone. *J Mol Cell Biol* **11**, 524–530.
21 Chen YH, Dey R & Chen L (2010) Crystal structure of the p53 core domain bound to a full consensus site as a self-assembled tetramer. *Structure* **18**, 246–256.
22 Oliner JD, Saiki AY & Caenepeel S (2016) The role of MDM2 amplification and overexpression in tumorigenesis. *Cold Spring Harb Perspect Med* **6**, a026336.
23 Buesoramos CE, Yang Y, Deleon E, Mccown P, Stass SA & Albitar M (1993) The human Mdm-2 oncogene is overexpressed in leukemias. *Blood* **82**, 2617–2623.
24 Prokocimer M, Molchadsky A & Rotter V (2017) Dysfunctional diversity of p53 proteins in adult acute myeloid leukemia: projections on diagnostic workup and therapy. *Blood* **130**, 699–712.
25 Colombo E, Martinelli P, Zamponi R, Shing DC, Bonetti P, Luzi L, Volorio S, Bernard L, Pruneri G, Alcalay M *et al.* (2006) Delocalization and destabilization of the Arf tumor suppressor by the leukemia-associated NPM mutant. *Cancer Res* **66**, 3044–3050.
26 Ando K, Tsushima H, Matsuo E, Horio K, Tominaga-Sato S, Imanishi D, Imaizumi Y, Iwanaga M, Itonaga H, Yoshida S *et al.* (2013) Mutations in the nucleolar phosphoprotein, nucleophosmin, promote the expression of the oncogenic transcription factor MEF/ELF4 in leukemia cells and potentiates transformation. *J Biol Chem* **288**, 9457–9467.
27 Kurki S, Peltonen K & Laiho M (2004) Nucleophosmin, HDM2 and p53 – players in UV damage incited nucleolar stress response. *Cell Cycle* **3**, 976–979.
28 Ianni A, Kumari P, Tarighi S, Simonet NG, Popescu D, Guenther S, Hölper S, Schmidt A, Smolka C, Yue S *et al.* (2021) SIRT7-dependent deacetylation of NPM promotes p53 stabilization following UV-induced genotoxic stress. *Proc Natl Acad Sci USA* **118**, e2015339118.
29 Lee C, Smith BA, Bandyopadhyay K & Gjerset RA (2005) DNA damage disrupts the p14ARF-B23 (nucleophosmin) interaction and triggers a transient subnuclear redistribution of p14ARF. *Cancer Res* **65**, 9834–9842.
30 Schuster K, Fan LY & Harris LC (2007) MDM2 splice variants predominantly localize to the nucleoplasm mediated by a COOH-terminal nuclear localization signal. *Mol Cancer Res* **5**, 403–412.
31 Brodska B, Kracmarova M, Holoubek A & Kuzelova K (2017) Localization of AML-related nucleophosmin mutant depends on its subtype and is highly affected by its interaction with wild-type NPM. *PLoS One* **12**, e0175175.
32 Lambert B & Buckle M (2006) Characterisation of the interface between nucleophosmin (NPM) and p53: potential role in p53 stabilisation. *FEBS Lett* **580**, 345–350.
33 Pauker MH, Hassan N, Noy E, Reicher B & Barda-Saad M (2012) Studying the dynamics of SLP-76, Nck, and Vav1 multimolecular complex formation in live human cells with triple-color FRET. *Sci Signal* **5**, rs3.
34 Fried S, Reicher B, Pauker MH, Eliyahu S, Matalon O, Noy E, Chill J & Barda-Saad M (2014) Triple-color FRET analysis reveals conformational changes in the WIP-WASp actin-regulating complex. *Sci Signal* **7**, ra60.
35 Eckenstaler R & Benndorf RA (2021) A combined acceptor photobleaching and donor fluorescence lifetime imaging microscopy approach to analyze multi-protein interactions in living cells. *Front Mol Biosci* **8**, 635548.
36 Lakowicz JR (2006) Principles of Fluorescence Spectroscopy. 3rd edn. Springer, New York, NY.

37 Lee HH, Kim HS, Kang JY, Lee BI, Ha JY, Yoon HJ, Lim SO, Jung G & Suh SW (2007) Crystal structure of human nucleophosmin-core reveals plasticity of the pentamer-pentamer interface. *Proteins* **69**, 672–678.
38 Holoubek A, Herman P, Sykora J, Brodska B, Humpolickova J, Kracmarova M, Gaskova D, Hof M & Kuzelova K (2018) Monitoring of nucleophosmin oligomerization in live cells. *Methods Appl Fluoresc* **6**, 035016.
39 Lambert TJ (2019) FPbase: a community-editable fluorescent protein database. *Nat Methods* **16**, 277–278.
40 Roth J, Dobbelstein M, Freedman DA, Shenk T & Levine AJ (1998) Nucleo-cytoplasmic shuttling of the hdm2 oncoprotein regulates the levels of the p53 protein via a pathway used by the human immunodeficiency virus rev protein. *EMBO J* **17**, 554–564.
41 Falini B, Brunetti L & Martelli MP (2015) Dactinomycin in NPM1-mutated acute myeloid leukemia. *N Engl J Med* **373**, 1180–1182.
42 Zucenka A, Vaitekenaite V, Maneikis K, Pileckyte R, Trociukas I, Peceliunas V & Griskevicius L (2021) Venetoclax, actinomycin D and low dose cytarabine for relapsed or refractory acute myeloid leukemia in clinical practice setting. *Blood* **138**, 3422.
43 Tzaridis T, Milde T, Pajtler KW, Bender S, Jones DT, Muller S, Wittmann A, Schlotter M, Kulozik AE, Lichter P *et al.* (2016) Low-dose actinomycin-D treatment re-establishes the tumoursuppressive function of P53 in RELA-positive ependymoma. *Oncotarget* **7**, 61860–61873.
44 Sasinkova M, Holoubek A, Otevrelova P, Kuzelova K & Brodska B (2018) AML-associated mutation of nucleophosmin compromises its interaction with nucleolin. *Int J Biochem Cell Biol* **103**, 65–73.
45 Bertwistle D, Sugimoto M & Sherr CJ (2004) Physical and functional interactions of the Arf tumor suppressor protein with nucleophosmin/B23. *Mol Cell Biol* **24**, 985–996.
46 Lee DH & Goldberg AL (1998) Proteasome inhibitors: valuable new tools for cell biologists. *Trends Cell Biol* **8**, 397–403.
47 Milner J & Medcalf EA (1991) Cotranslation of activated mutant P53 with wild-type drives the wild-type P53 protein into the mutant conformation. *Cell* **65**, 765–774.
48 Okorokov AL, Sherman MB, Plisson C, Grinkevich V, Sigmundsson K, Selivanova G, Milner J & Orlova EV (2006) The structure of p53 tumour suppressor protein reveals the basis for its functional plasticity. *EMBO J* **25**, 5191–5200.
49 Rajagopalan S, Huang F & Fersht AR (2011) Single-molecule characterization of oligomerization kinetics and equilibria of the tumor suppressor p53. *Nucleic Acids Res* **39**, 2294–2303.
50 Ma L, Wagner J, Rice JJ, Hu W, Levine AJ & Stolovitzky GA (2005) A plausible model for the digital response of p53 to DNA damage. *Proc Natl Acad Sci USA* **102**, 14266–14271.
51 Gaglia G, Guan Y, Shah JV & Lahav G (2013) Activation and control of p53 tetramerization in individual living cells. *Proc Natl Acad Sci U S A* **110**, 15497–15501.
52 Lomax ME, Barnes DM, Hupp TR, Picksley SM & Camplejohn RS (1998) Characterization of p53 oligomerization domain mutations isolated from Li-Fraumeni and Li-Fraumeni like family members. *Oncogene* **17**, 643–649.
53 Marston NJ, Jenkins JR & Vousden KH (1995) Oligomerization of full-length P53 contributes to the interaction with Mdm2 but not Hpv E6. *Oncogene* **10**, 1709–1715.
54 Katz C, Low-Calle AM, Choe JH, Laptenko O, Tong D, Joseph-Chowdhury JSN, Garofalo F, Zhu Y, Friedler A & Prives C (2018) Wild-type and cancer-related p53 proteins are preferentially degraded by MDM2 as dimers rather than tetramers. *Gene Dev* **32**, 430–447.
55 Ziemer MA, Mason A & Carlson DM (1982) Cell-free translations of proline-rich protein mRNAs. *J Biol Chem* **257**, 11176–11180.
56 Rizzo MA, Springer GH, Granada B & Piston DW (2004) An improved cyan fluorescent protein variant useful for FRET. *Nat Biotechnol* **22**, 445–449.
57 Davidson M & Piston D. Addgene plasmid # 54604; http://n2t.net/addgene:54604; RRID:Addgene_54604
58 Koushik SV, Chen H, Thaler C, Puhl HL 3rd & Vogel SS (2006) Cerulean, Venus, and VenusY67C FRET reference standards. *Biophys J* **91**, L99–L101.
59 Vogel S. Addgene plasmid # 27793; http://n2t.net/addgene:27793; RRID:Addgene_27793
60 Lahav G, Rosenfeld N, Sigal A, Geva-Zatorsky N, Levine AJ, Elowitz MB & Alon U (2004) Dynamics of the p53-Mdm2 feedback loop in individual cells. *Nat Genet* **36**, 147–150.
61 Alon U & Lahav G. Addgene plasmid # 53962; http://n2t.net/addgene:53962; RRID:Addgene_53962
62 Davidson M & Piston D. Addgene plasmid # 54742; http://n2t.net/addgene:54742; RRID:Addgene_54742
63 Herman P, Holoubek A & Brodska B (2019) Lifetime-based photoconversion of EGFP as a tool for FLIM. *Biochim Biophys Acta Gen Subj* **1863**, 266–277.
64 Davison AC & Hinkley DV (1997) Bootstrap Methods and Their Application. Cambridge University Press, Cambridge.